G05.89-0.39 – Another Ultracompact HII Region Under the Looking Glass

M. Feldt[1], B. Stecklum[2], Th Henning[1], T.L. Hayward[3]

[1] Astrophysical Institute & University Observatory Jena, Schillergäßchen 3, D-07745 Jena, Germany
[2] Thuringian State Observatory Tautenburg, Sternwarte 5, D-07778 Tautenburg, Germany
[3] Center for Radiophysics and Space Research, Cornell University, Ithaca, NY 14853, U.S.A.

1. Introduction

Ultracompact HII regions (UCHIIs) are the most obvious signposts of young, massive stars($M \geq 8M_{\odot}$). Such stars reside deeply embedded in molecular cloud cores hidden from optical view. Their birth is indicated by UCHIIs caused by the ionization of the dense ambient matter (Henning 1990, Churchwell 1991). In recent years, it has been realized that massive stars spend a considerable fraction of their lifetime in the UCHII stage (Wood & Churchwell 1989). Beech & Mitalas (1994) even suggest that the most massive stars may remain invisible during their *whole* main-sequence phase.

Many problems arise in the context of UCHIIs and many theories have been proposed to explain their nature – The bow-shock model by Van Buren et al. (1990), which explains the cometary structure of UCHIIs as well as accounts for the so-called lifetime problem and the hypothesis about UCHIIs being evaporating circumstellar disks by Hollenbach et al. (1994) which also explains the longevity of the UCHII phase are only two examples. It is also still unclear whether UCHIIs are usually powered by single stars or by a cluster inside – an important question with respect to in what multiplicities massive stars usually form.

Due to the high extinction towards these regions, UCHIIs can only be observed at wavelengths from the infrared longwards. To effectively address the above questions it is also necessary to achieve the highest possible resolutions. Now that adaptive optics systems have become widely available, the resolutions of earlier VLA observations, primarily the studies of Wood & Churchwell (1989) and Kurtz, Churchwell & Wood (1994), can be matched in the near infrared domain.

Table 1: Summary of Observations

Date	λ	Tel./Instr.	FOV[a]	PSF FWHM	Ref. Star[b]	Limiting Mag.[c]
1992 Aug	11.7 μm	200" Hale/SpectroCam10	$16\farcs2$	$1\farcs1$	αLyr (0.00)	5.0[c]
1995 Aug	H/K'	ESO 3.6 (ADONIS/SHARP2)	$13''$	$0\farcs5/0\farcs4$[d]	Y4338 (5.68/5.42)	21.1/19.6
1996 Mar	1.3 mm	ESO SEST (Bolo)	–	$23''$	Uranus	–
1996 May	L	ESO 3.6 (ADONIS/COMIC)	$12\farcs8$	$0\farcs52$	–	–
1996 Oct	Q	ESO 2.2 (MANIAC)	$43\farcs5$	$1\farcs5$	ηSgr (-1.74)	5.0
1998 May	10.6 μm/12.8 μm	ESO 3.6 m (TIMMI)	$43''$	$1\farcs1$	ηSgr(-1.65 / -1.74)	4.9 / 4.9
1998 Jul	2.164 μm (Brγ)	ESO 2.2 m/IRAC2b	$130''$	$1\farcs5$	HD169588 (8.71)	14.6

[a] Field of view for single frames

[b] With brightness given in magnitudes for the observed wavelength

[c] Derived from background noise for point sources with given PSF

[d] Seeing was $1\farcs0$ during the observations, the resolution is improved by the adaptive optics correction

Table 1: Summary of observations.

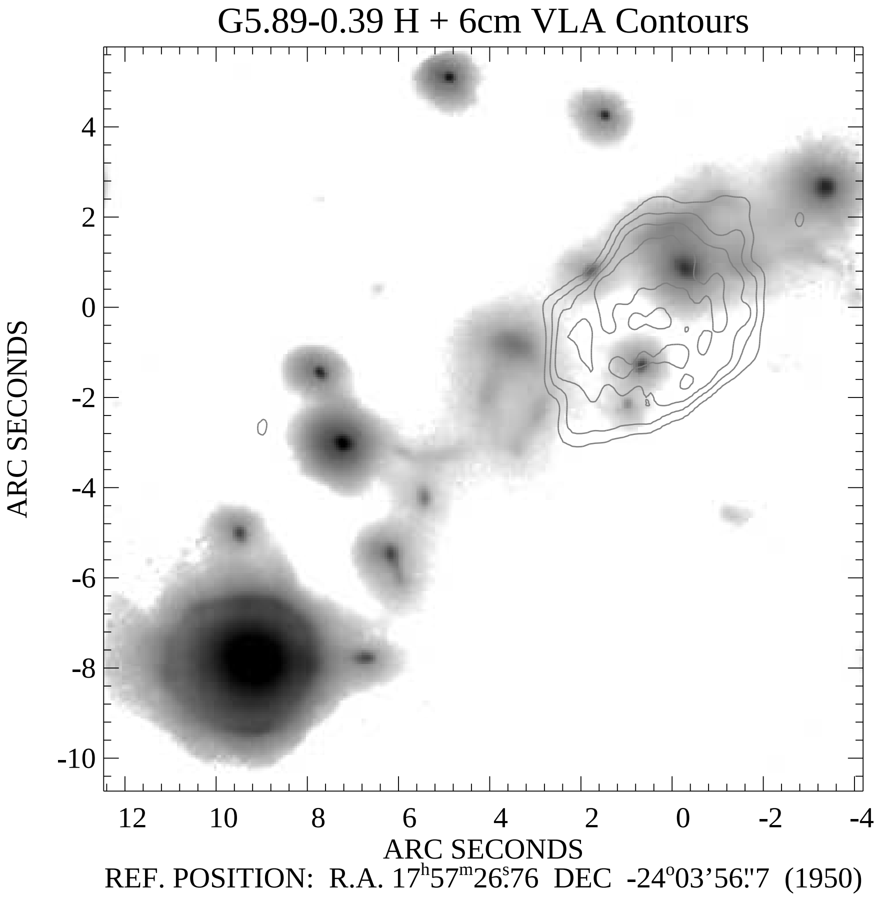

Figure 1: H image of G5.89. The logarithmic gray scale ranges from $0.04\,\mathrm{mJy}/\square''$to $31\,\mathrm{mJy}/\square''$. To enhance the visibility of details, a combination of deconvolved and original image is shown, both were subject to a maximum entropy filtering algorithm (see text). The contours are from the 6 cm VLA map by WC89, levels are 2, 4, 6, and 8 times the sigma level of 5 mJy/beam.

Our example of G05.89-0.39 (G5.89) appears to be an UCHII slowly appearing at the rim of a very dense, massive cloud still obscuring half the region from view. The UCHII itself appears to be of spherically symmetric geometry – apart from a breach of symmetry in north-south direction which might be responsible for outflow activity. Thus we are able to explain most of its properties with a very simple model.

2. Observations

2.1 The AO System ADONIS

ESO's adaptive optics system ADONIS is a high-order correction system for the near- to mid-infrared. It has two Shack-Hartmann Sensors (EBCCD for reference stars fainter than $m_V = 8\,\mathrm{mag}$ and Reticon for brighter reference stars) with 7×7 sub-apertures each. The deformable mirror has 52 actuators and the system can run at a correction rate of up to 60 Hz (The wavefront sensors are evaluated at a speed up to 400 Hz). A maximum of 20 Zernike modes can be corrected. Under optimum conditions (seeing $\approx 0''.7$, guide star $m_V = 5\,\mathrm{mag}$), ADONIS can reach a Strehl ratio of 0.52 and a FWHM of the point-spread-function (PSF) of $0''.15$ in K, i.e. the image is essentially diffraction limited. A detailed performance report is given in Bonaccini et al. (1997). Under more typical conditions like our observations (seeing $1''.0$, guide star $m_V = 12\,\mathrm{mag}$), the system can still reach a FWHM of $0''.4$. The image is not

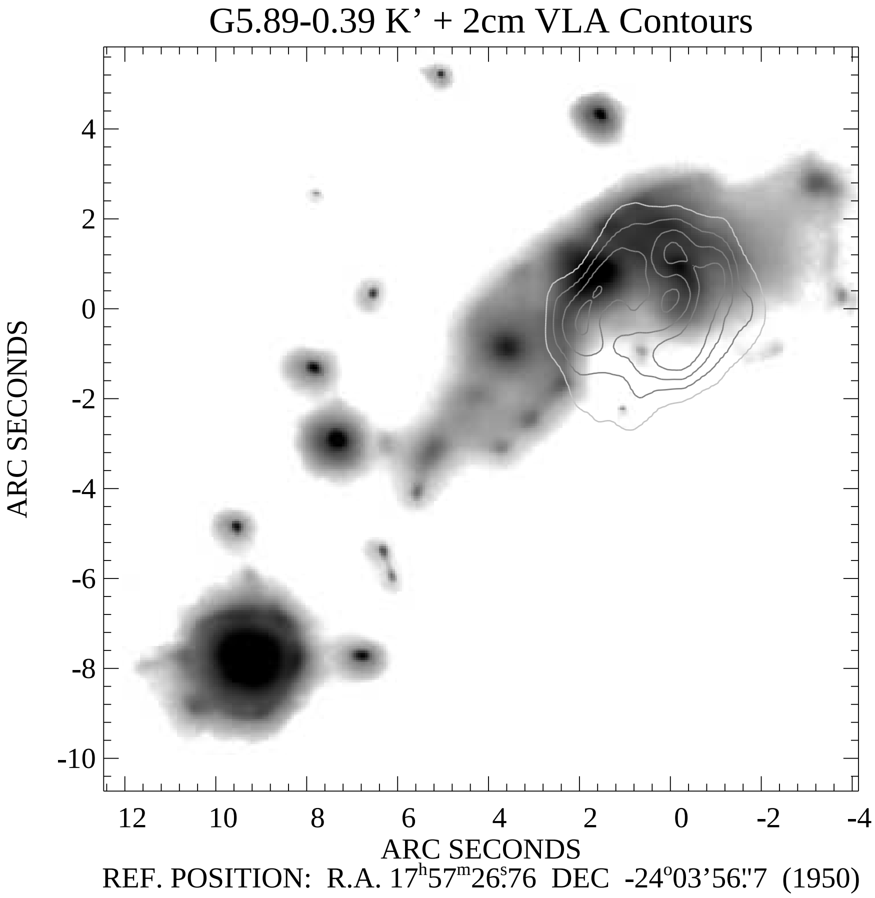

Figure 2: K' image of G5.89. The logarithmic gray scale ranges from $0.39\,\mathrm{mJy}/\Box''$to $31\,\mathrm{mJy}/\Box''$. To enhance the visibility of details, a combination of deconvolved and original image is shown, both were subject to a maximum entropy filtering algorithm (see text). The contours are from the 2 cm VLA map by WC89, levels are 2, 4, 6, 8, and 10 times the sigma level of 0.03 Jy/beam.

diffraction limited then and has to be post-processed if one wants to remove the extended halo of point sources.

We observed G5.89 using ADONIS in H and K' in August 1995 using the SHARP-II camera. In each band, a mosaic of three frames was obtained resulting in a total integration time of 400 to 600 s, depending on the location in the frame. During the observations, the seeing was $1''$, the high-order adaptive optics correction improved the full-width half-maximum (FWHM) of the point spread function (PSF) to $0\farcs4$ in K' and $0\farcs5$ in H. All frames were subject to standard bad-pixel removal, flat fielding, and dark-frame subtraction processes before being combined in the resulting images. For calibration purposes, images were taken of the UKIRT standard Y4338. Post processing was done by applying a maximum-likelihood deconvolution (Lucy 1974) using the guide star as PSF. An L band image was obtained in May 1996 using the COMIC camera in combination with ADONIS. 432 frames of 3 s integration time each were combined in the resulting image. As the original goal was to do polarimetry, these were obtained at four different positions of the polariser. Because the signal-to-noise ratio proved too low, all frames were combined in the resulting image. The mean Strehl given by the ADONIS software was 0.075, the PSF FWHM in the image is $0\farcs52$ while the seeing monitor reported a seeing of $1\farcs2$. No photometric calibration was done for this image.

2.2 Supplementary Observations

ADONIS can provide high-resolution images, but it has a limited field of view and wavelength range. There-

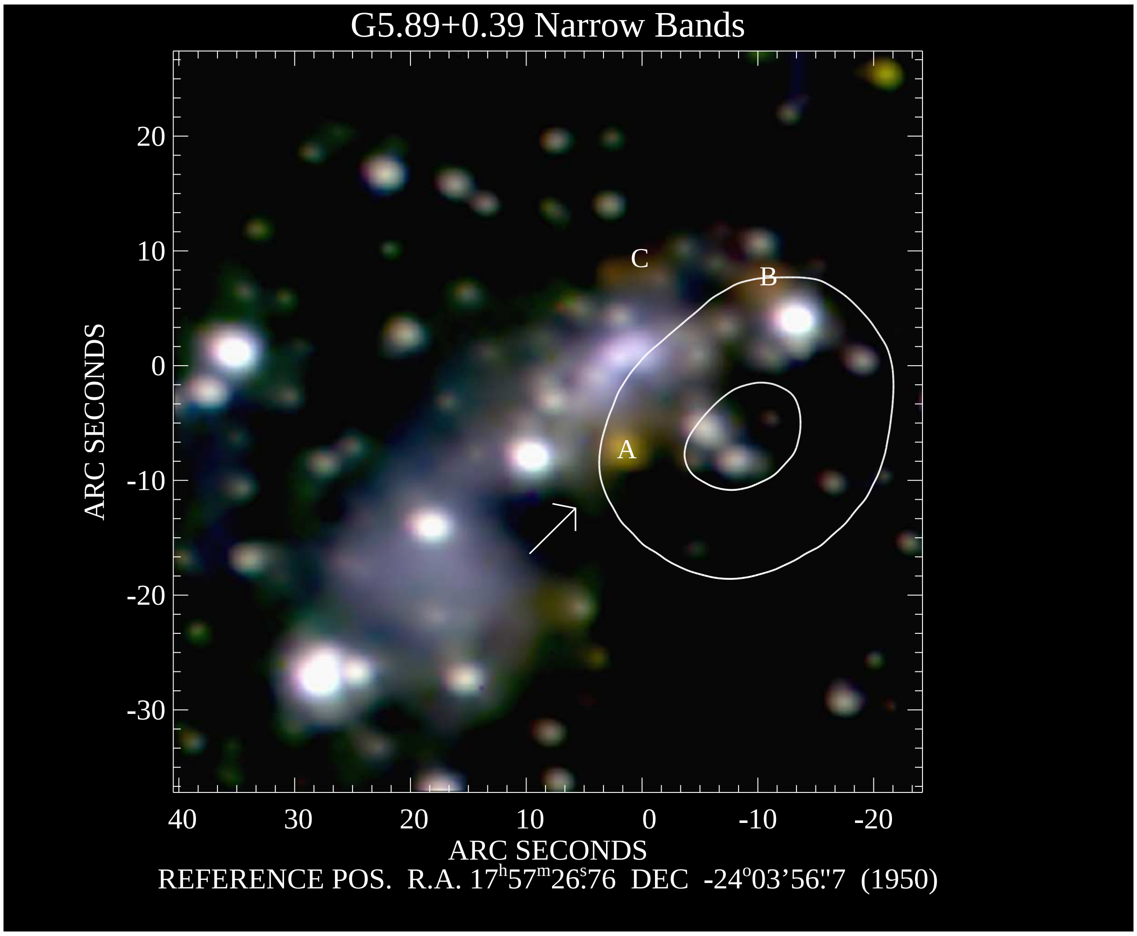

Figure 3: Colour coded image of G5.89 taken in three narrow band filters. Red represents light emitted in the H_2(1–0)S1 line, green is narrow band continuum emission and blue Brγ. The white contour lines mark the 50% and the 90% level of the 1.3 mm emission after the free-free contribution was subtracted. The marks A, B, and C denote locations where H_2 flux was measured (see text). The arrow points to the beginning of the cloud rim.

fore, complementary observations in the mid-infrared and at 1.3 mm were performed which are summarised in Tab. 1.

3. G5.89-0.39

Figures 1 and 2 show the high resolution near-infrared images. These show highly reddened, extended emission around the position of G5.89 which is marked by the radio contour lines. The extraordinary resolution of these images allows to see several distinct sources embedded in the diffuse background, e.g. the two single sources in the southern part of the radio shell which are the least reddened sources in the area and therefore probably belong to the foreground. The importance of this identification becomes clear with a glance at Fig. 3, which shows the wide field narrow band image of the source. Now a large structure of clouds is visible immediately south of the bluish arc of G5.89 (at the reference position), indicated by the lack of field stars and brownish rims. From a comparison with Figs. 1 and 2 it now seems that the rim of this cloud which is obviously cutting G5.89 in half and stretching towards the southeast (its end is marked by the arrow) appears as a chain of unresolved yet embedded sources in the K' band image. This is probably due to the structure of this rim with varying reflection and ionization properties. The measurement with the SEST tells us that the 1.3 mm emission has its origin also slightly offset from G5.89 and probably inside the main body of the cloud. When subtracting the free-free contribution (predicted from a 2 cm map by Wood & Churchwell, 1989)from the 1.3 mm map we get the result presented in Fig. 3 as contours. The measured

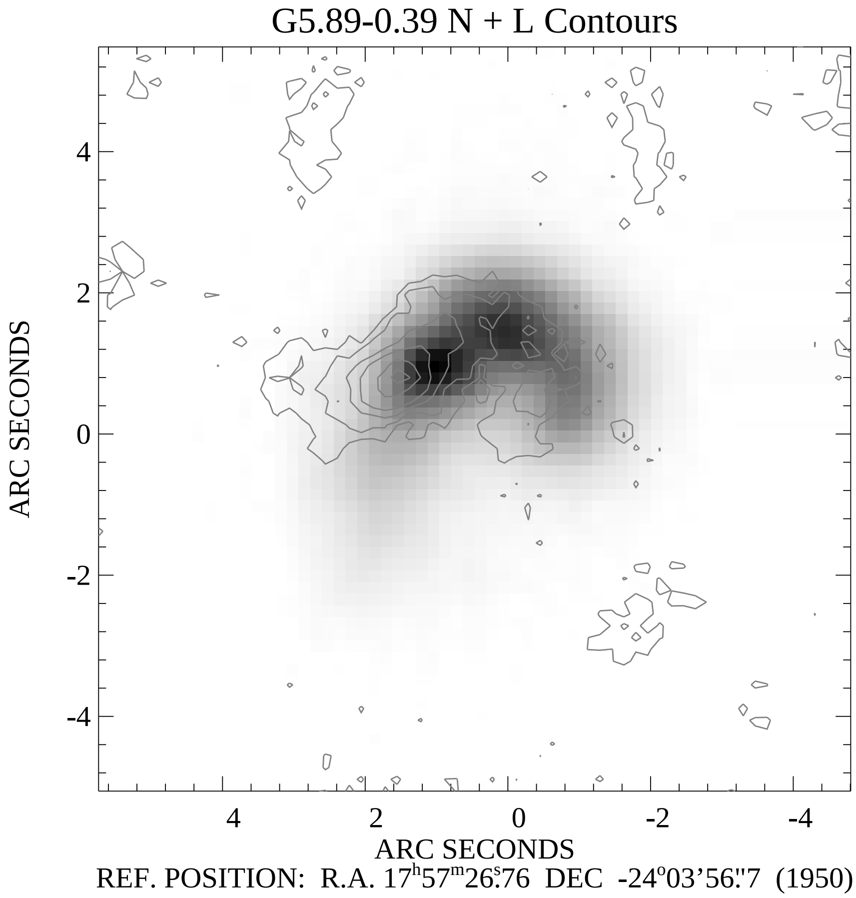

Figure 4: N Band image of G5.89. The linear gray scale ranges from 150 mJy/□″to 15 Jy/□″. Contours are from our L band image. Arbitrary levels are 3, 6, 9, 12, and 18 times the sigma level in the image.

remaining flux of 8.5 Jy and size of 16″ across tells us that enough dust is present in the cloud (7.5 $M_\odot$) to provide sufficient extinction to render the southern part of G5.89 invisible even in the Q band (A_Q = 55 mag). Thus, the massive foreground cloud can easily explain the shape of G5.89 and its constance from the near to the mid infrared. We believe it to be highly probable that G5.89 developed out of this cloud and is now contributing to its destruction as is the star at position (+9″,-8″), which is also identified as an early type star from the colour information.

This interpretation also means that G5.89 is of mainly spherical geometry as clearly seen in the radio maps (Figs. 1 and 2). This appearance can be reproduced by a spherical shell of dust with an inner, dust-free cavity. Such a model was proposed by Churchwell, Wolfire & Wood (1990), the inner rim of the dust shell appears as a bright arch at all infrared wavelengths then, which is consistent with our observations. The radio (and clearly also the NIR) maps show however a breach of symmetry in form of a "channel" in north-south direction. This direction is consistent with most outflow observations of the source (Harvey & Forveille 1988; Acord et al., 1997) . It is also confirmed by our finding of 2 H_2 line emission areas north and south of G5.89, marked "A" and "C" in Fig. 3. The locations of our H_2 emission regions are close to the $C^{34}S$ line wing centroid position found by Cesaroni et al. (1991). As the modelling requires a large, dust-free inner cavity, a driving mechanism for the outflow similar to that suggested in Yorke & Welz (1996) were outflows are driven by the photo evaporation of disks surrounding massive young stars might be applicable. Whether a disk is (or was) present inside G5.89 or whether only material from the inner edge of the dust shell is being photo-evaporated, we cannot decide from these observations.

Apart from this breach, the mid-infrared observations show that in the L, N, and Q band the source appears ring-shaped (Figs. 4 & 5). The same is true for our other observations, except for the 1.3 mm map, where the reso-

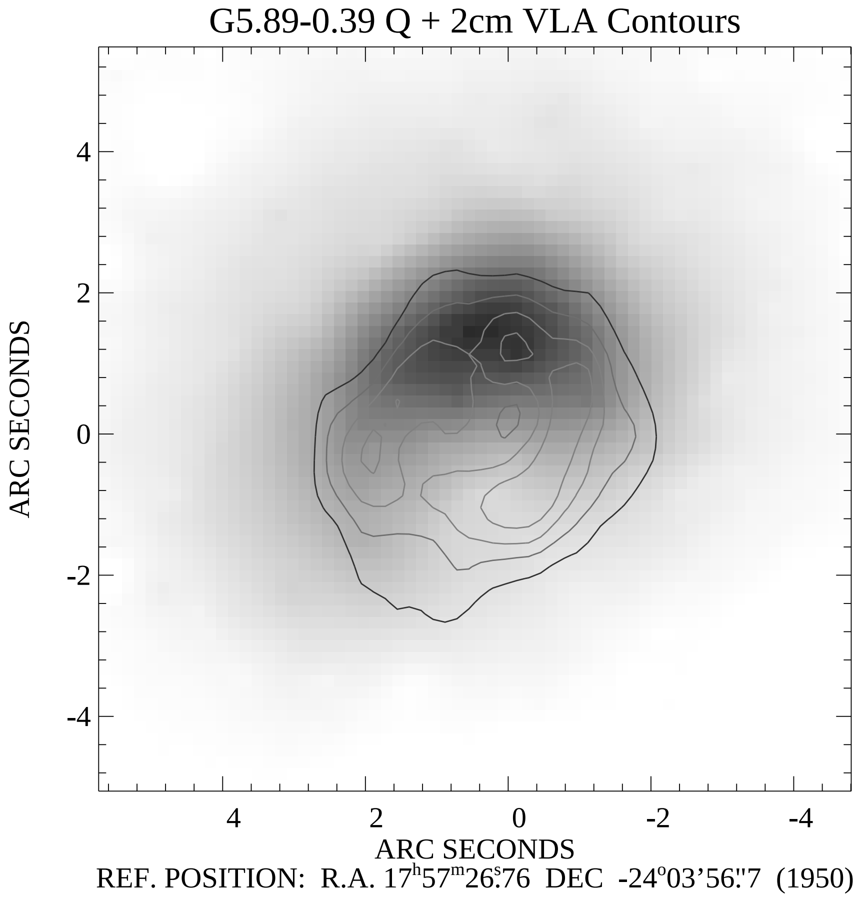

Figure 5: Q Band image of G5.89. The linear gray scale ranges from 5 mJy/□″to 38 mJy/□″. The contours are the same as in Fig. 2.

lution is too coarse to derive the shape. It appears however, that the 1.3 mm emission is only partly due to free-free emission, one half being obviously caused by the foreground cold dust. We will not discuss the model of the source which we made as a consequence of these results here in detail, but like to refer the reader to a forthcoming paper on this issue (Feldt et al. 1998b).

4. Benefits from AO Observations

The ADONIS images clearly offer a superb resolution which is needed for proper identification of the infrared with optical and radio sources. Astrometric calibration was achieved by aligning the infrared frames with the digitized sky survey after all. However, from this work it becomes clear that AO observations have also some drawbacks and need to be complemented by large-field, "conventional" observations. In Feldt et al. (1998a) we demonstrated the usefulness of AO observations for the ultracompact HII region G45.45+0.06 by identifying 15 point sources inside the VLA map by Wood & Churchwell (1989), eight of which could be identified as massive stars. This identification, and indeed the detection of these sources against the extended background was only possible because of the high resolution achieved by the AO. On the other hand, this time we have a source that is 2.4 times less distant. Thus, with the same resolution we are now looking at a single source in detail. It turns out, that spatial information on *extended* emission is much harder to extract from the AO images than on point sources. This is demonstrated by the simple simulation shown in Fig 6. It also becomes obvious form a comparison of Figs. 2 and 3: The rim of the cloud is only partially seen in the high resolution images and the H_2 feature A is completely undetected there.

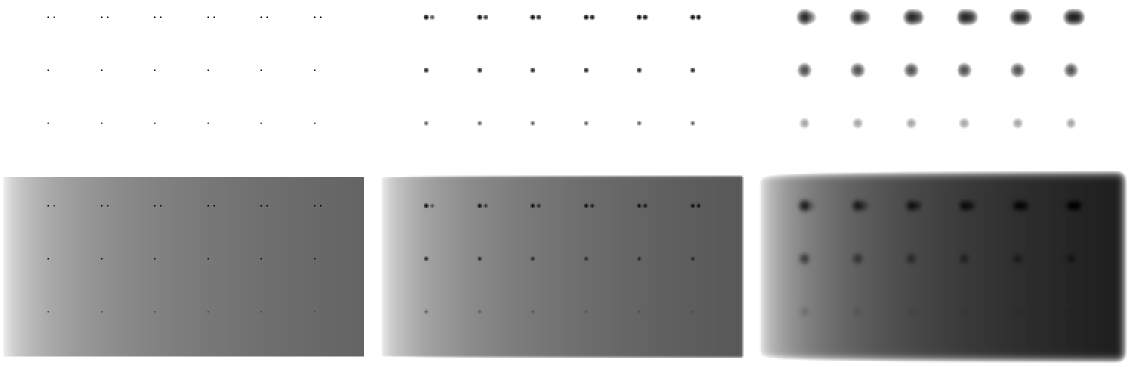

Figure 6: Demonstration of observations with different resolutions. **A**: Input pattern of a typical situation in ultracompact HII regions. Several point sources, represented by delta peaks, are configured in double stars of decreasing contrast and 0."5 separation (upper row). Second and third row represent weaker stars. The lower half repeats this situation embedded in a varying, extended background. **B**: The configuration convolved with the theoretical PSF (Gaussian approximation) of a 3.6 m telescope. **C**: The pattern convolved with the PSF of an exceptionally good seeing of 0."5. It becomes clear, that in the latter case many of the point sources go undetected against the background. However, observations which are targeted at the background can draw benefits from the situation.

Obviously, the sensitivity towards extended emission suffers from the use of AO. This needs to be compensated by longer integration times if one needs both informations.

6 Acknowledgements

The Authors are grateful for the help of Patrice Bouchet during the ADONIS observations. We also thank Markus Buchner or providing the narrow band data and reading this manuscript.

6 References

Acord J.M., Walmsley C.M., Churchwell E., 1997, ApJ 475, 693
Beech, M. & Mitalas, R., 1994, ApJS, 95, 517
Bonaccini D., Prieto E., Corporon P., et al., 1997, SPIE 3126-78
Cesaroni R., Walmsley C.M., Kömpe C., Churchwell E., 1991, A&A 252, 278
Churchwell E., Wolfire M.G.,Wood D.O.S., 1990, ApJ354, 257
Draine B.T., Lee H.M., 1984, ApJ 285, 89
Feldt M., Stecklum B., Henning Th., et al., 1998a, A&A 340, in press
Feldt M., Stecklum B., Henning Th., Hayward T.L., Launhardt R., 1998b, A&A, submitted
Harvey P.M., Forveille T., 1988, A&A 197, L19
Hollenbach, D. et al. , 1994, ApJ 428, 654
Kurtz, Churchwell & Wood, 1994, ApJS 91, 659
Van Buren et al. 1990, ApJ 353, 570
Wood D.O.S., Churchwell E., 1989, ApJS 69, 831
Yorke H.W., Welz A., 1996, A&A 315, 555